nature photonics

ARTICLES

PUBLISHED ONLINE: 21 SEPTEMBER 2015 | DOI: 10.1038/NPHOTON.2015.181

Non-collinear generation of angularly isolated circularly polarized high harmonics

Daniel D. Hickstein[1]*, Franklin J. Dollar[1], Patrik Grychtol[1], Jennifer L. Ellis[1], Ronny Knut[1], Carlos Hernández-García[1,2], Dmitriy Zusin[1], Christian Gentry[1], Justin M. Shaw[3], Tingting Fan[1], Kevin M. Dorney[1], Andreas Becker[1], Agnieszka Jaroń-Becker[1], Henry C. Kapteyn[1], Margaret M. Murnane[1] and Charles G. Durfee[1,4]

We generate angularly isolated beams of circularly polarized extreme ultraviolet light through the first implementation of non-collinear high harmonic generation with circularly polarized driving lasers. This non-collinear technique offers numerous advantages over previous methods, including the generation of higher photon energies, the separation of the harmonics from the pump beam, the production of both left and right circularly polarized harmonics at the same wavelength and the capability of separating the harmonics without using a spectrometer. To confirm the circular polarization of the beams and to demonstrate the practicality of this new light source, we measure the magnetic circular dichroism of a 20 nm iron film. Furthermore, we explain the mechanisms of non-collinear high harmonic generation using analytical descriptions in both the photon and wave models. Advanced numerical simulations indicate that this non-collinear mixing enables the generation of isolated attosecond pulses with circular polarization.

The high harmonic generation (HHG) process can be used to produce attosecond bursts of extreme ultraviolet (EUV) and soft X-ray light using tabletop-scale lasers[1–3], enabling numerous applications, including nanoscale imaging[4–8], studies of nanoscale energy transport[9] and element-specific probes of charge and spin dynamics on the femtosecond timescale[10–14]. HHG produces EUV light through an ionization-and-recollision process[15], and because recollision does not occur when an atom is irradiated with circularly polarized light, for many years it was believed to be impossible to generate circularly polarized EUV light by the HHG process. This precluded many powerful techniques (such as EUV and soft X-ray magnetic circular dichroism (MCD) and photoelectron circular dichroism) from being implemented on the tabletop. Consequently, there have been numerous experimental[16–18] and theoretical[19,20] efforts to directly produce circularly polarized harmonics using a single driving laser beam, but such efforts have yielded only elliptically polarized high harmonics.

In a recent breakthrough, Fleischer *et al.*[21] experimentally demonstrated that HHG driven by two collinear beams with counter-rotating circular polarization can directly generate EUV light with circular polarization, as was predicted theoretically[22,23]. Moreover, phase matching of collinear circularly polarized HHG is remarkably robust, providing a bright source of EUV light and thereby enabling tabletop EUV MCD measurements[24]. However, collinear circularly polarized HHG requires driving lasers at different wavelengths[21,24,25], which increases the experimental complexity. Furthermore, collinear HHG produces a pulse train of three linearly polarized attosecond bursts per laser cycle, where the polarization rotates 120° between each burst[22] (and sums to produce circular polarization at the sample). Consequently, if very short-duration driving pulses were used to produce an isolated attosecond pulse, it would have linear (or in some cases elliptical[26]) polarization.

In this work we demonstrate a new approach: non-collinear circularly polarized HHG (NCP-HHG), in which circularly polarized high harmonics are generated using crossed beams of counter-rotating circularly polarized driving lasers (Fig. 1a). NCP-HHG offers several key benefits not found in other HHG methods (Supplementary Fig. 1). First, circularly polarized harmonics can be generated using a single-colour driving laser, maximizing the photon energies obtained. Second, angularly isolated circularly polarized beams of both left and right helicity can be generated at the same wavelength, enabling precision differential measurements of circular dichroism at a single wavelength in a single exposure. Third, by adjusting the crossing angle of the driving laser beams, the different harmonic orders can be angularly separated without the need for a spectrometer (Fig. 1a, Supplementary Fig. 2). Finally, the harmonics are naturally separated from the driving laser beams, allowing a fragile sample to be placed directly into the EUV beams without the need for filters, thus significantly increasing the usable HHG flux. Here, we use the NCP-HHG source to perform an EUV MCD measurement of a 20-nm-thick iron sample, confirming that the EUV beams are circularly polarized with opposite helicity and demonstrating that the brightness and stability of the source are sufficient to measure the ultrafast dynamics of magnetic materials.

We explain the mechanisms of non-collinear HHG using both intuitive physical models as well as advanced numerical calculations. In the photon picture (Fig. 1b), we show that the NCP-HHG method is governed by simple selection rules, allowing the emission angles of EUV emission to be calculated analytically. Using a simple wave-mixing model (Fig. 1c), we find that the circularly polarized high harmonics are generated by driving fields that are, in fact, locally linear. The linearity of the field experienced by each atom enables the optimal cutoff photon energies of linearly polarized HHG to be realized for circularly

[1]JILA – Department of Physics, University of Colorado and NIST, Boulder, Colorado 80309, USA. [2]Grupo de Investigación en Óptica Extrema, Universidad de Salamanca, Salamanca E-37008, Spain. [3]Electromagnetics Division, National Institute of Standards and Technology, Boulder, Colorado 80305, USA. [4]Department of Physics, Colorado School of Mines, Golden, Colorado 80401, USA. *e-mail: danhickstein@gmail.com

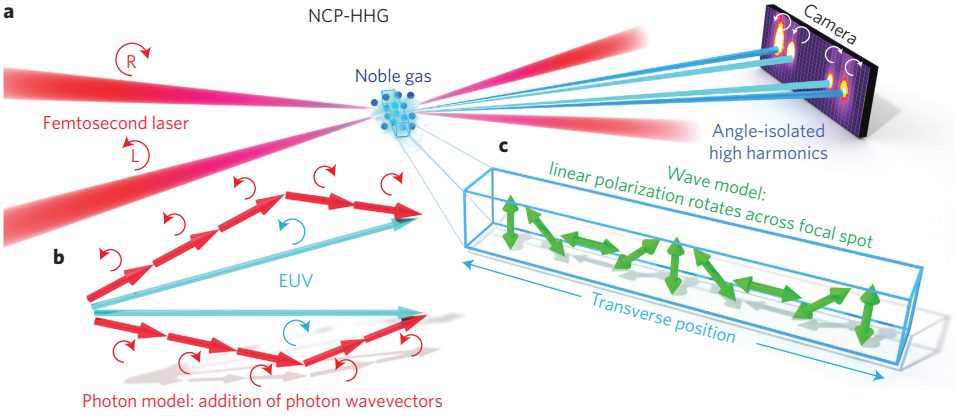

Figure 1 | Non-collinear circularly polarized high harmonic generation (NCP-HHG). a, In the NCP-HHG experiment, two counter-rotating circularly polarized femtosecond laser pulses are focused into a noble gas (Xe, Ar or Ne) to produce both left and right circularly polarized beams of EUV light via HHG. The detector shows experimental data for NCP-HHG driven by 267 nm lasers, where EUV beams at 23 eV (inner) and 14 eV (outer) emerge at different angles, well separated from the driving laser beams. **b**, In the photon model, the output direction of each harmonic follows the simple vector addition of the wavevectors for each absorbed photon. **c**, In the wave model, the two circularly polarized beams sum to yield an electric field that exhibits linear polarization, which rotates as a function of the transverse position across the laser focus, producing a 'rotating polarization grating' that generates circular polarization in the far field.

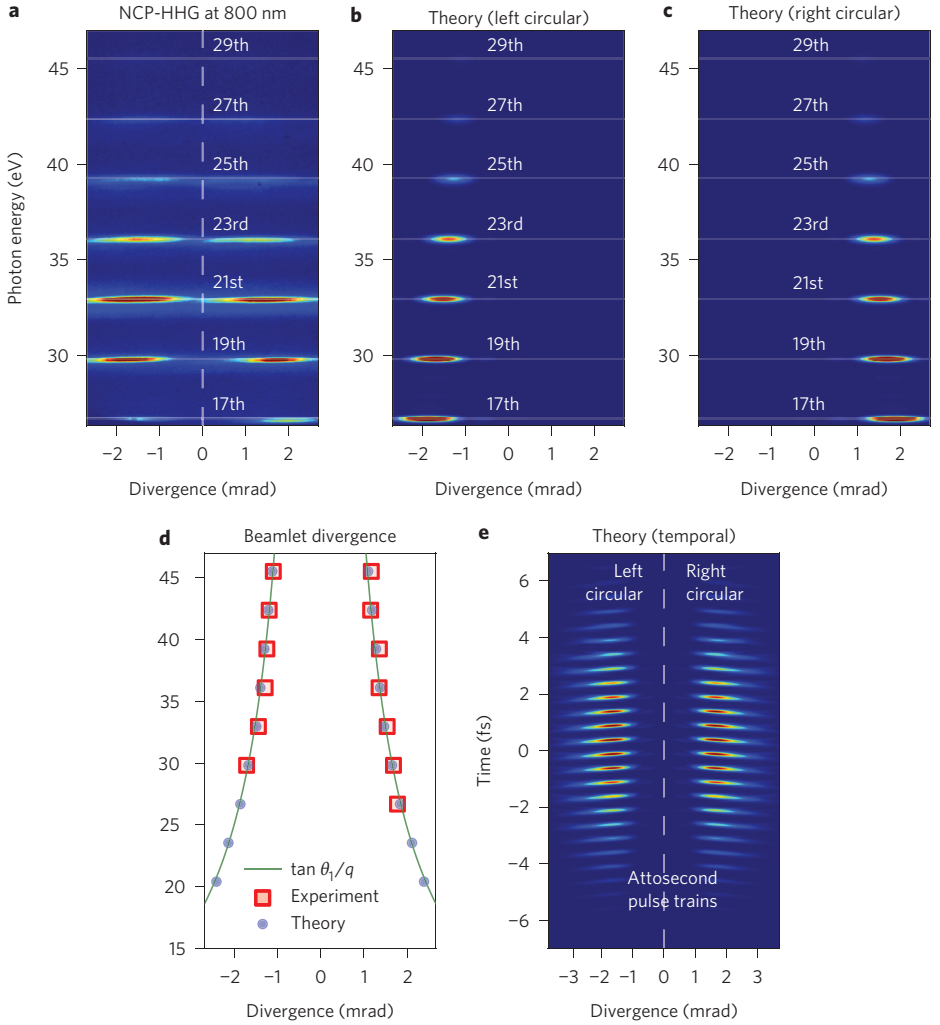

Figure 2 | NCP-HHG using two 800 nm pulses. a, The EUV output of the NCP-HHG process is recorded after passing through a spectrometer, which disperses the harmonics in the vertical direction. Each harmonic consists of two beams, one at an angle left of the centreline (left circular polarization) and one to the right of the centreline (right circular polarization). **b**,**c**, Numerical HHG simulations driven by 4.3-cycle 800 nm laser pulses demonstrate that the left beamlets are left circularly polarized and the right beamlets are right circularly polarized. **d**, The divergence of each harmonic order q follows conservation of momentum, which predicts that the angle of harmonic emission, θ_q, is related to the crossing angle of the two laser beams, θ_1, by $\tan\theta_q = \pm\tan\theta_1/q$. **e**, The temporal structure of the harmonic emission is a pulse train of many circularly polarized attosecond bursts.

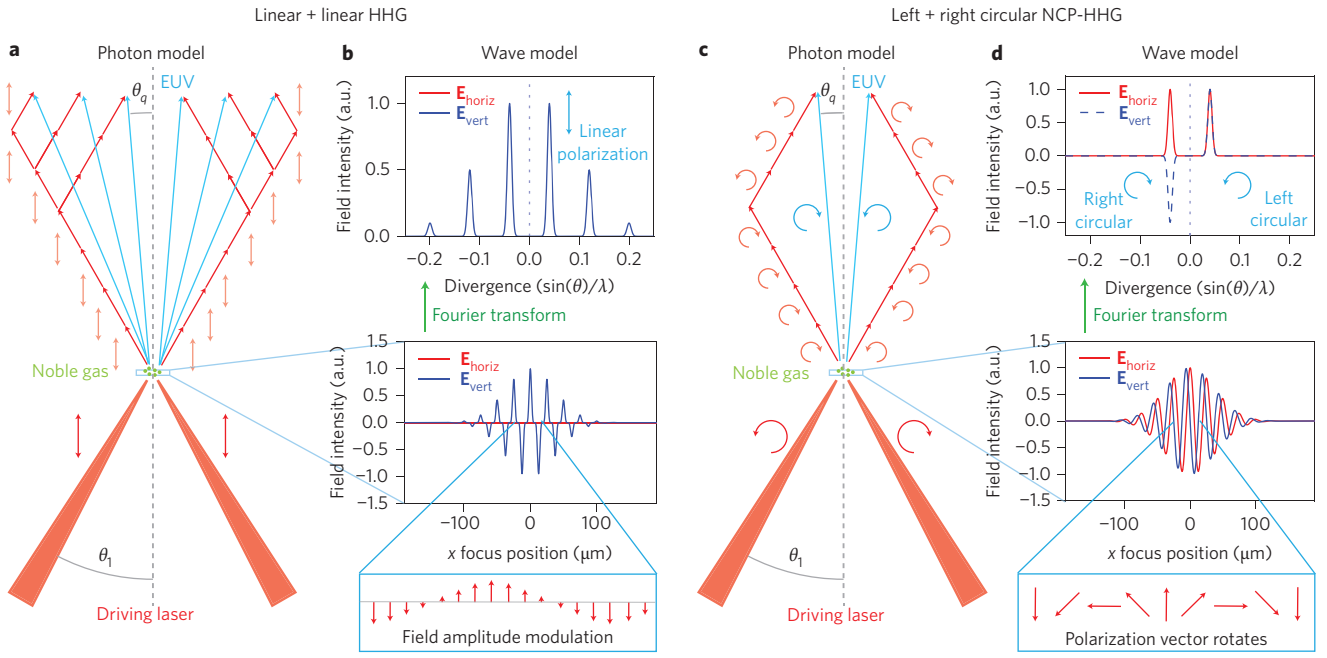

Figure 3 | Photon and wave models of non-collinear HHG. a, For the mixing of linearly polarized laser beams, the only constraint is that the total number of absorbed photons is odd. This allows many combinations of photons for any given harmonic (in this case the seventh harmonic) and results in EUV beams emerging at many different angles. **b**, In the wave model, two-beam mixing produces an amplitude-modulated grating at the focus, which produces multiple peaks in the far field. **c**, For counter-rotating circularly polarized beams, conservation of spin angular momentum requires that $n_R = n_L \pm 1$, restricting the output to only two beams for each harmonic. **d**, In the wave picture, the left and right circular mixing produces linear polarization that rotates as a function of the transverse focal position. This rotation is purely sinusoidal and consequently produces just two output beams, one left circularly polarized and one right circularly polarized.

polarized HHG. Finally, numerical simulations show that this non-collinear generation method extends to generating an isolated attosecond burst. To our knowledge, this is the first method capable of producing an isolated attosecond burst with circular polarization.

NCP-HHG

To generate circularly polarized high harmonics in a non-collinear geometry, two tightly focused, counter-rotating 45 fs laser pulses were overlapped in a gas jet of noble gas (xenon, argon or neon), where the HHG process took place (Methods). The generated EUV beams propagated in vacuum and passed through an aluminium filter (200-nm-thick, 20–72 eV transmission window), which blocked any scattered visible light. The EUV beams were then dispersed by an imaging spectrometer and recorded with an X-ray charge-coupled device (CCD) camera. Harmonics were generated only when the beams were overlapped both temporally and spatially. Otherwise, the HHG mechanism was suppressed due to the circular polarization of the individual laser beams. Two EUV beams were produced for each odd harmonic order, with one circularly polarized beam propagating to the right of the centreline and the other (with opposite helicity) to the left (Fig. 2a).

When two 800 nm driving beams were used to generate harmonics in argon gas, the resulting high harmonic photon energies reached the 29th harmonic order (45 eV). In xenon gas, only 100 μJ in each driving laser beam was sufficient to generate high harmonics, demonstrating that the NCP-HHG method is easily scalable to current multi-kHz laser systems. Numerical simulations (Methods) confirmed, for the case of perfect alignment, that the harmonics are fully circularly polarized with opposite helicity (Fig. 2b,c).

The nature of the harmonic emission can be adjusted by changing the wavelength of the driving laser. When two 400 nm pulses were used to drive the process in argon (Supplementary Figs 3 and 4), a single high-flux ($\sim 2 \times 10^8$ photons per pulse) harmonic at 22 eV was observed, and two harmonics (22 and 28 eV) were generated when neon was used as the HHG medium. When 267 nm beams were used to drive the NCP-HHG process, angularly separated beams at 14 and 23 eV were generated (Fig. 1a, Supplementary Fig. 2). Note that the NCP-HHG method produces circularly polarized beams that are separated by helicity and harmonic order, in contrast to methods such as attosecond lighthouse[27,28] or non-collinear optical gating[29,30], which produce angularly separated attosecond pulses with linear polarization (Supplementary Section 1).

In NCP-HHG, the emission angle of the two EUV HHG beams is a small fraction of the crossing angle of the driving laser beams, resulting in harmonics that are angularly separated from the driving laser. The divergence angle θ_q of the harmonic beams decreases with increasing harmonic order q and closely follows the trend $\tan\theta_q = \pm\tan\theta_1/q$, where θ_1 is the crossing half-angle of the driving laser beams (Fig. 2d). The angular dependence of the harmonic emission can be explained by a simple photon model that takes into consideration the conservation of parity, linear momentum and angular momentum (Fig. 3a,c) for the photons absorbed and emitted in the HHG process. Because of parity conservation, the number of photons absorbed to generate a given harmonic $n = n_+ + n_-$ must be odd (n_+ and n_- refer to the number of photons absorbed from each of the two pump beams). Conservation of linear momentum dictates that the output momentum of the harmonic photon, k, is related to the momentum of the input photons ($\mathbf{k}_+$ and $\mathbf{k}_-$) by simple vector addition $\mathbf{k} = n_+\mathbf{k}_+ + n_-\mathbf{k}_-$. As these are the only two requirements for linearly polarized beams, the non-collinear mixing of two linearly polarized beams generates harmonics at a variety of divergence angles (Fig. 3a), including both angles smaller than the crossing angle of the driving beams (sum frequency generation) and angles larger than the crossing angle of the driving beams (difference frequency generation)[31].

In contrast, in the case of counter-rotating (left and right) circularly polarized driving beams, conservation of spin angular

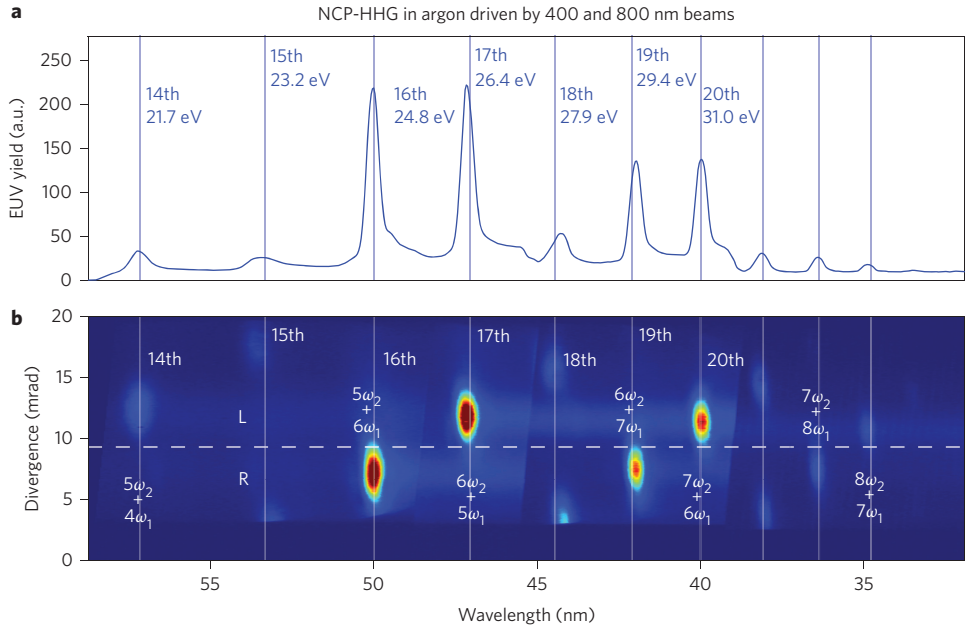

Figure 4 | NCP-HHG driven by different frequency driving lasers (400 and 800 nm). a, The angle-integrated harmonic spectrum reveals the 'left, right, missing' pattern seen in collinear circularly polarized HHG[21,24]. a.u., arbitrary units. **b**, In contrast to collinear generation, non-collinear HHG generates one helicity in one direction and the opposite helicity in the other direction. The low intensity peaks at the 15th, 18th and 21st harmonic orders are a result of the slight ellipticity of the driving laser beams.

momentum adds an additional constraint on the allowed combinations, namely that $n_R = n_L \pm 1$. This selection rule, combined with conservation of momentum[21,32,33], dictates that a given harmonic can only produce two beams (Fig. 3c). The output beam directions for harmonic order q follow $\tan\theta_q = \pm\tan\theta_1/q$, in agreement with the experiment and numerical simulations (Fig. 2d). Significantly, all the harmonics are directed away from the pump beams and, provided the initial crossing angle is sufficiently large and the harmonic divergence sufficiently small, individual harmonics can be separated without using a diffraction grating (Fig. 1a and Supplementary Fig. 2).

Further insight into the non-collinear HHG process can be gained by considering non-collinear mixing within a wave model. The crossing of two linearly polarized beams (Fig. 3b) produces an interference pattern at the focal plane and, because the high harmonic yield is highly nonlinear with respect to the driving field, there are many diffracted orders in the far field. In contrast, the crossing of two circularly polarized counter-rotating beams (Fig. 3d) does not produce an interference pattern at the crossing plane because the polarizations are orthogonal. However, provided that the amplitudes of the beams are equal, the combined polarization is locally linear. Because the relative phase of the beams varies across the focal spot, the orientation of the linear polarization also varies (Figs 1c and 3d):

$$\mathbf{E}(x) = E_0 e^{-x^2/\omega^2}\left[\,\hat{\mathbf{x}}\cos(k_1 x \sin\theta_1) - \hat{\mathbf{y}}\sin(k_1 x \sin\theta_1)\,\right]$$

where x is the spatial coordinate across the focal spot and ω determines the beam waist. The linear polarization that rotates across the focal spot forms a 'rotating polarization grating' (Figs 1c and 3d), which is the key to NCP-HHG.

In the interaction region, the atoms emit high harmonic radiation polarized in the direction of the local (linearly polarized) fundamental field. We consider the propagation of the horizontal and vertical components of the source polarization separately. The horizontally polarized component can be treated as a plane wave that is phase modulated with a spatial cosine pattern. In the far field, there will be only two diffracted orders (+1, −1), with no zero-order (d.c.) component (Fig. 3d, top). Similarly, the vertically polarized component is also phase modulated, but with a sine spatial pattern. From Fourier optics, the 90° spatial phase shift of this emitting pattern leads to a ±90° phase shift of the ±1 diffracted orders. Thus, the combined fields in the two diffracted directions will be circularly polarized with opposite helicity. The angle of diffraction for the qth harmonic is determined by the modulation period of the fundamental. In the paraxial approximation, $\sin\theta_q = \sin\theta_1/q$, which is in agreement with the photon model when θ_1 is small.

The locally linear field in the $\omega + \omega$ NCP-HHG method differentiates this technique from $\omega + 2\omega$ mixing schemes[21,24], which produce a trefoil (three-leaf clover) shaped field. Because of the two-dimensional nature of the electric field in the $\omega + 2\omega$ method, the field-driven electron wave packet is driven back to the ion from different directions as a function of time[22,23,34], and the kinetic energy of the electron at recollision is lower than a linear field at ω. The mechanism at play in the $\omega + \omega$ non-collinear scheme is qualitatively distinct, as each atom experiences a linearly polarized driving field. This is advantageous, because the same single-atom physics of linear HHG apply, allowing high photon energies to be produced.

An additional benefit of the NCP-HHG method is that the generated harmonics are angularly separated from the driving laser (Fig. 1a). This separation does not occur for single-beam or collinear HHG, where the harmonics co-propagate with the driving laser(s) after the interaction region. In this case, optically dense (typically aluminium) filters must be placed between the HHG source and the sample to block the driving laser and prevent sample damage. The filters can attenuate much of the EUV (often by a factor of 20 or more) and require that the sample be placed far from the interaction region (typically 40 cm or more), allowing the harmonic beam to diverge significantly. In contrast, using NCP-HHG, we demonstrate that a fragile sample (in this case, a single human hair) can be placed just 1 cm from the interaction region without damage (Supplementary Fig. 4d). In this geometry, the sample experiences an unusually high EUV intensity (on the order of GW cm^{-2}) without the need for filters, mirrors or gratings. Considering the high expense and low efficiency of optics in the

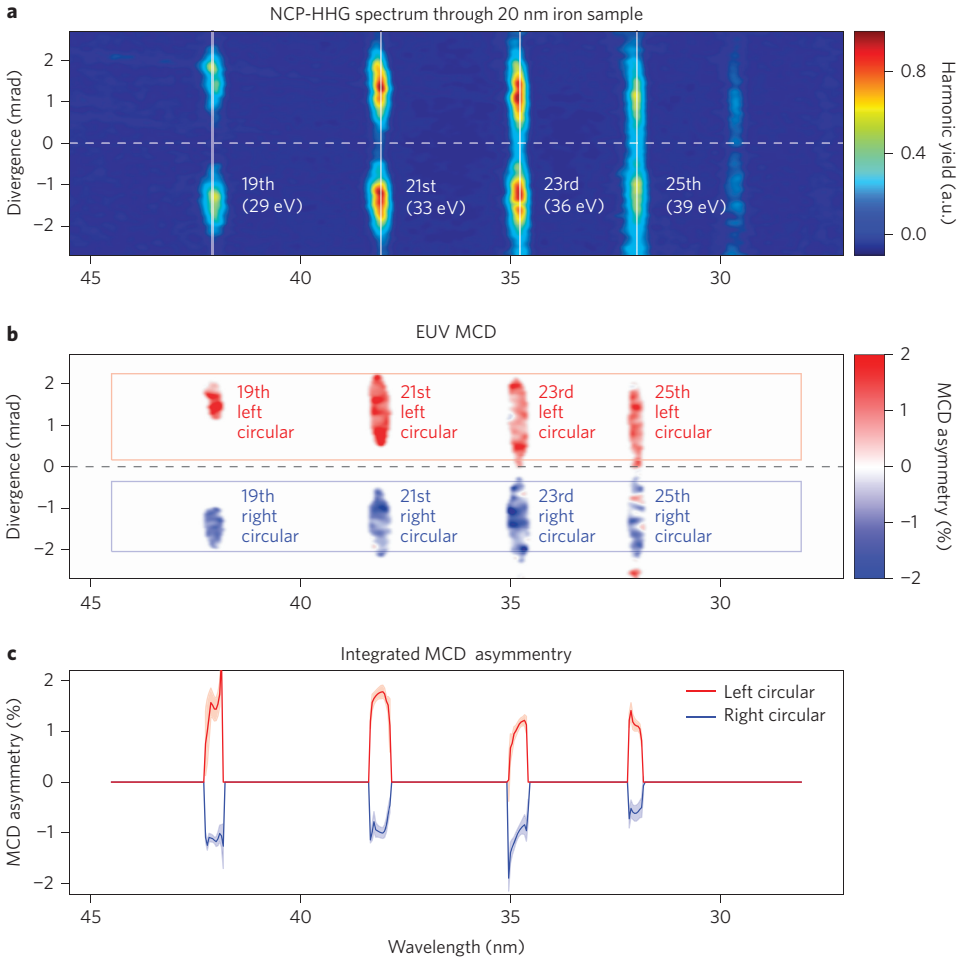

Figure 5 | EUV MCD of an iron film. a, Spectrum of circularly polarized harmonics generated from 800 nm beams focused in argon and transmitted through a 20-nm-thick iron sample at 45° incidence. **b**, MCD asymmetry ($A_{MCD} = (I_+ - I_-)/(I_+ + I_-)$) between opposing magnetization states in the iron sample. As expected, left circularly polarized harmonics (red) display opposite dichroism to right circularly polarized harmonics (blue). **c**, Integrated MCD asymmetry and 95% confidence interval demonstrate that the dichroism is antisymmetric for the left and right polarizations and is in good quantitative agreement with the predicted magneto-optical contrast based on the available synchrotron data[39,40] (Supplementary Section 6).

EUV spectral region, this simplification of the apparatus constitutes a substantial advantage.

Non-collinear HHG phase matching

Experimentally, the NCP-HHG method generates a high flux of EUV photons, which is remarkable considering that the length of the interaction region is limited when compared to single-beam or collinear HHG. Fortunately, the decreased length of the interaction region is partially compensated by a modification of the phase-matching conditions that arises due to the non-collinear geometry. Although the microscopic (single-atom) physics of the circularly polarized non-collinear HHG method is identical to that for single-beam linearly polarized HHG, macroscopically the crossed-beam mixing adds a geometric component to the phase-matching equation. Specifically, for non-collinear mixing of plane waves, we take the projection of the k-vector of the pump beams along the direction of the output harmonic beam:

$$\Delta k = n_L k_1 \cos(\theta_1 - \theta_q) + n_R k_1 \cos(\theta_1 + \theta_q) - k_q$$

where each k includes the bound and free electron contributions to the refractive index of the medium at the corresponding frequency. The effective refractive index of the harmonic light is close to unity, but the refractive index at the fundamental is greater than the one for bound electrons and decreases in the presence of free electrons. Provided that the free electron density is below a critical value[3,35], the target density can be increased to achieve phase matching, just as it can for single-beam HHG. This situation holds for any crossing angle, because the bound and free electron contributions to the refractive index are both multiplied by the cosine angular factor.

Thus, as a result of phase matching, the optimal pressure for harmonic generation increases dramatically with increasing crossing angle. This increase in pressure tends to compensate for the decreased length of the interaction region that is imposed by the non-collinear geometry. As a result, NCP-HHG can reach high flux levels as long as sufficient gas pressures can be provided. In this initial experiment, the maximum achievable pressure in the interaction region was limited to ~1 kPa by the capacity of the vacuum pump, limiting phase matching to the EUV range. In the future, high-pressure gas targets should allow NCP-HHG to extend to soft X-ray wavelengths.

Non-collinear HHG with different frequency driving lasers

The circularly polarized non-collinear HHG process is not limited to mixing two beams of the same frequency. We demonstrated this by generating circularly polarized harmonics by mixing 400 and 800 nm beams in argon (Fig. 4). The angle-integrated spectrum (Fig. 4a) of the EUV emission exhibits the familiar 'left, right, missing' pattern seen in collinear circularly polarized HHG, where

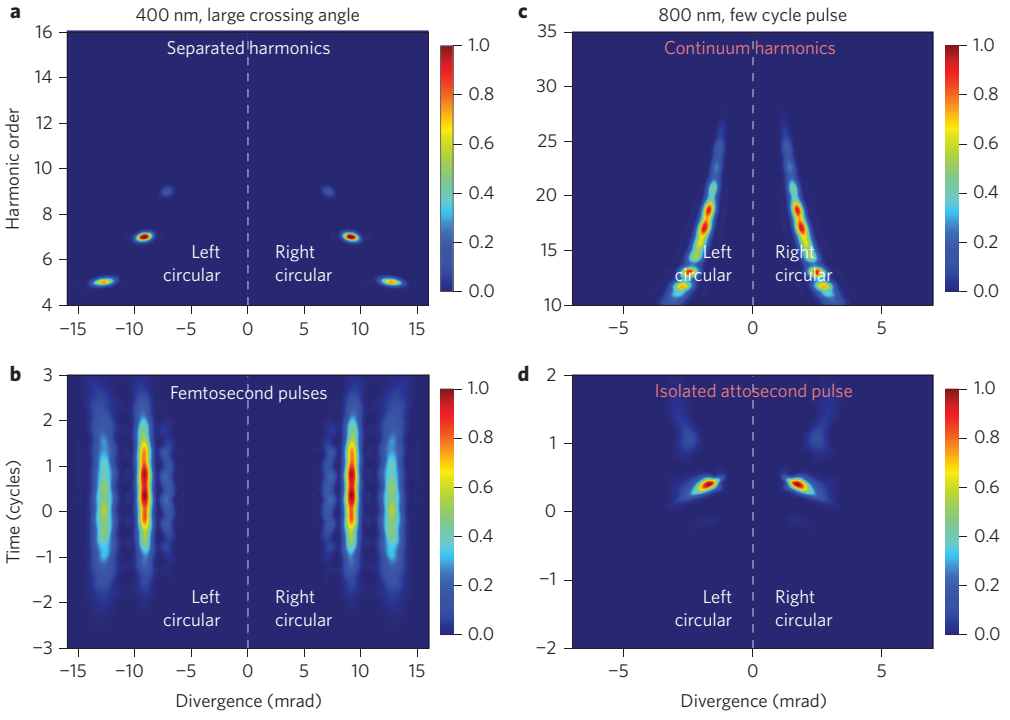

Figure 6 | Numerical simulations reveal additional capabilities of the NCP-HHG method. a, When driven by 4.3-cycle, 400 nm pulses at a large (64 mrad) crossing angle, angularly separated harmonics are produced, obviating the need for a spectrometer. **b**, In the time domain, each of these harmonics manifests as an angularly separated pulse with a timescale similar to the driving laser. **c**, When driven with 1.1-cycle 800 nm pulses (32 mrad crossing angle), supercontinuum harmonics are produced. **d**, In the time domain, the EUV emission manifests as two isolated attosecond pulses, one left circularly polarized and one right circularly polarized. Colour scales are in linear arbitrary units. Each panel is normalized separately.

the left circular harmonics are separated in frequency from the right circular harmonics, and every third harmonic is suppressed[21,23,24,36,37]. Furthermore, the angle-resolved spectrum (Fig. 4b) reveals that the left circularly polarized harmonics are emitted in one direction, and the right circular harmonics in the opposite direction. Moreover, in contrast to non-collinear mixing at the same frequency, where the harmonics are grouped around the centreline of the pump beams, the harmonics generated from the mixing of 400 and 800 nm beams are displaced towards the direction of the 400 nm output beam because of momentum conservation (Supplementary Section 4).

EUV MCD measurements

One of the most powerful uses for ultrashort pulses of circularly polarized EUV and soft X-ray light is the study of femtosecond dynamics of magnetic materials using EUV and X-ray MCD[38]. In these measurements, the magnetic state of a material is probed by the dichroic absorption of circularly polarized light, which can provide both elemental specificity and distinction between the spin and orbital contributions to the atomic magnetic moment. Because the dichroic absorption scales linearly with the degree of circular polarization (Methods), MCD can also provide a rigorous measurement of the ellipticity and helicity of the EUV light. The dichroism can be measured either by comparing the difference in absorption between the left and right circularly polarized light or by using a magnetic field to flip the sample magnetization. We performed an EUV MCD measurement by switching the magnetic field applied to a 20-nm-thick iron film and comparing the transmitted EUV intensities $I_{\pm}$ for opposing magnetization directions, as expressed by the MCD asymmetry $A_{\mathrm{MCD}} = (I_+ - I_-)/(I_+ + I_-)$.

Experimentally, the MCD asymmetry is readily apparent, even in the two-dimensional image (Fig. 5b), and clearly demonstrates that the two beams exhibit opposite helicity. Angular integration (Fig. 5c) provides a quantitative estimate of the MCD asymmetry of ~1.5% in the range of 29–39 eV. To our knowledge, there is no experimental measurement of the MCD contrast (or magneto-optical constants) of iron in this energy range, but synchrotron data at slightly higher photon energies are available[39,40]. The trend of the data indicates that the MCD asymmetry in the range of our measurement is less than 2% (Supplementary Fig. 6). Thus, our measurement of ~1.5% asymmetry confirms that the EUV light generated by the NCP-HHG process has a high degree of circular polarization. Furthermore, this EUV MCD measurement demonstrates that the NCP-HHG source is a practical tool for measuring ultrafast magnetic dynamics. The data presented in Fig. 5 represent 30 min of averaging, but an adequate measure of MCD asymmetry can be acquired in 2 min (Supplementary Fig. 7), opening the door to time-resolved pump–probe studies of femtosecond-resolved magnetic dynamics.

Future capabilities investigated with numerical simulations

Numerical simulations of HHG including propagation (Methods) provide insight into further capabilities of the NCP-HHG method. First, experimentally, the harmonics could only be angularly separated when using 267 nm driving lasers due to the low pressure in the interaction region (Fig. 1). However, simulations predict that similar separation can be achieved at longer driving laser wavelengths and higher harmonic photon energies. For example, simulations indicate that 400 + 400 nm-driven NCP-HHG at a 64 mrad crossing angle will produce harmonics that are completely separated angularly (Fig. 6a). The situation is similar for longer wavelengths, but the required crossing angle becomes larger. The separation of the harmonics allows for spectroscopic experiments such as X-ray transient absorption spectroscopy and MCD to be completed without a spectrometer to disperse the

harmonics, a distinct advantage considering the high expense, low efficiency and temporal dispersion of gratings in the EUV and soft X-ray regions. In this case, the HHG process itself serves as the dispersive grating (Fig. 3d). Of course, where separation of the harmonic beams is not desirable, a small crossing angle can be used to achieve good overlap of the harmonic orders, and the NCP-HHG method can still serve as a practical source of circularly polarized high harmonic light.

Simulations also provide clear insight into the temporal structure of the EUV emission. When all the harmonics are angularly separated (Fig. 6a), the EUV beams emerge as single long pulses (Fig. 6b), with a temporal duration somewhat shorter than that of the driving laser (that is, a several-femtosecond pulse). When the harmonics are angularly overlapped, the standard 'attosecond pulse train' is generated, which consists of numerous attosecond bursts (Fig. 2e). However, with few-cycle driving pulses, angularly dispersed supercontinuum harmonics are generated (Fig. 6c). In the time domain, this manifests as an isolated attosecond pulse of circularly polarized EUV light (Fig. 6d). Though previous theoretical works have proposed the generation of isolated circularly polarized attosecond pulses using exotic conditions, such as very intense terahertz fields[41], to our knowledge, the NCP-HHG method is the first experimentally realized method that is capable of producing isolated attosecond pulses with circular polarization.

Discussion

Looking forward, the NCP-HHG method is poised to enable breakthrough probes of ultrafast dynamics. When driven with few-cycle pulses, simulations indicate that the NCP-HHG method will produce two circularly polarized isolated attosecond pulses, one propagating to the left and one to the right. This geometry naturally lends itself to an attosecond pump–attosecond probe experiment, which could be implemented using a single 'split-mirror' focusing optic to adjust the temporal delay. Because the NCP-HHG method can eliminate the need for all other optics, gratings and filters, both the EUV intensity at the sample and the EUV flux at the detector could reach levels unprecedented in attosecond pump–attosecond probe experiments, potentially transforming these formidable experiments into commonplace techniques for probing the fastest processes in materials, molecules and atoms. Similarly, for imaging studies, refocusing the two beams of opposite helicity with a single optic will allow for new control over illumination, proving either separated right and left circular polarization, or a 'textured' linear polarization reproducing the rotating polarization pattern of the source. Furthermore, recent work has shown that high-intensity circularly polarized EUV pulses can be used to generate attosecond magnetic field pulses[42].

Here, we have demonstrated NCP-HHG for the first time, and have shown that this method generates bright circularly polarized EUV beams of both left and right helicity simultaneously. Owing to selection rules, the two helicities are angularly isolated, and each harmonic order is emitted at a different angle (Fig. 1), allowing the HHG process itself to serve as a spectrometer. Conveniently, the EUV light is well separated from the intense driving-laser beams. Using this new light source, we performed an EUV MCD measurement that confirmed the circular polarization of the EUV light and demonstrated that the flux and stability of the source are sufficient for real-world studies of femtosecond magnetic dynamics. Importantly, we demonstrated that the single-atom physics of the NCP-HHG process is identical to that of single-beam linearly polarized HHG, indicating that the NCP-HHG method can be extended to produce circularly polarized harmonics in the soft X-ray region by using mid-infrared driving lasers[43,44], produce high-flux EUV sources using ultraviolet driving lasers[45], and generate isolated attosecond pulses using few-cycle driving lasers[46].

Methods

Methods and any associated references are available in the online version of the paper.

Received 22 April 2015; accepted 21 August 2015; published online 21 September 2015; corrected online 7 October 2015

References

1. McPherson, A. *et al.* Studies of multiphoton production of vacuum-ultraviolet. *J. Opt. Soc. Am. B* **4,** 595–601 (1987).
2. Ferray, M. *et al.* Multiple-harmonic conversion of 1064 nm radiation in rare gases. *J. Phys. B* **21,** L31–L35 (1988).
3. Rundquist, A. *et al.* Phase-matched generation of coherent soft X-rays. *Science* **280,** 1412–1415 (1998).
4. Seaberg, M. D. *et al.* Ultrahigh 22 nm resolution coherent diffractive imaging using a desktop 13 nm high harmonic source. *Opt. Express* **19,** 22470–22479 (2011).
5. Seaberg, M. D. *et al.* Tabletop nanometer extreme ultraviolet imaging in an extended reflection mode using coherent Fresnel ptychography. *Optica* **1,** 39–44 (2014).
6. Adams, D. E., Wood, C., Murnane, M. M. & Kapteyn, H. C. Tabletop high harmonics illuminate the nano-world. *Laser Focus World* (4 May 2015); http://go.nature.com/6T1Wvi
7. Ravasio, A. *et al.* Single-shot diffractive imaging with a table-top femtosecond soft X-ray laser-harmonics source. *Phys. Rev. Lett.* **103,** 028104 (2009).
8. Miao, J., Ishikawa, T., Robinson, I. K. & Murnane, M. M. Diffractive imaging with coherent X-ray sources. *Science* **348,** 530–535 (2015).
9. Hoogeboom-Pot, K. M. *et al.* A new regime of nanoscale thermal transport: collective diffusion counteracts dissipation inefficiency. *Proc. Natl Acad. Sci. USA* **112,** 4846–4851 (2014).
10. Mathias, S. *et al.* Probing the timescale of the exchange interaction in a ferromagnetic alloy. *Proc. Natl Acad. Sci. USA* **109,** 4792–4797 (2012).
11. Turgut, E. *et al.* Controlling the competition between optically induced ultrafast spin-flip scattering and spin transport in magnetic multilayers. *Phys. Rev. Lett.* **110,** 197201 (2013).
12. Miaja-Avila, L. *et al.* Direct measurement of core-level relaxation dynamics on a surface-adsorbate system. *Phys. Rev. Lett.* **101,** 46101 (2008).
13. Beaurepaire, E., Merle, J.-C., Daunois, A. & Bigot, J.-Y. Ultrafast spin dynamics in ferromagnetic nickel. *Phys. Rev. Lett.* **76,** 4250–4253 (1996).
14. Bigot, J.-Y., Vomir, M. & Beaurepaire, E. Coherent ultrafast magnetism induced by femtosecond laser pulses. *Nature Phys.* **5,** 515–520 (2009).
15. Corkum, P. B. Plasma perspective on strong field multiphoton ionization. *Phys. Rev. Lett.* **71,** 1994–1997 (1993).
16. Zhou, X. *et al.* Elliptically polarized high-order harmonic emission from molecules in linearly polarized laser fields. *Phys. Rev. Lett.* **102,** 073902 (2009).
17. Lambert, G. *et al.* Towards enabling femtosecond helicity-dependent spectroscopy with high-harmonic sources. *Nature Commun.* **6,** 6167 (2015).
18. Ferré, A. *et al.* A table-top ultrashort light source in the extreme ultraviolet for circular dichroism experiments. *Nature Photon.* **9,** 93–98 (2015).
19. Yuan, K. J. & Bandrauk, A. D. Circularly polarized molecular high-order harmonic generation in H_2^+ with intense laser pulses and static fields. *Phys. Rev. A* **83,** 063422 (2011).
20. Yuan, K. J. & Bandrauk, A. D. Generation of circularly polarized attosecond pulses by intense ultrashort laser pulses from extended asymmetric molecular ions. *Phys. Rev. A* **84,** 023410 (2011).
21. Fleischer, A., Kfir, O., Diskin, T., Sidorenko, P. & Cohen, O. Spin angular momentum and tunable polarization in high-harmonic generation. *Nature Photon.* **8,** 543–549 (2014).
22. Milošević, D. B. & Becker, W. Attosecond pulse trains with unusual nonlinear polarization. *Phys. Rev. A* **62,** 011403(R) (2000).
23. Milošević, D. B., Becker, W. & Kopold, R. Generation of circularly polarized high-order harmonics by two-color coplanar field mixing. *Phys. Rev. A* **61,** 063403 (2000).
24. Kfir, O. *et al.* Generation of bright circularly-polarized extreme ultraviolet high harmonics for magnetic circular dichroism spectroscopy. *Nature Photon.* **9,** 99–105 (2015).
25. Fan, T. *et al.* Bright circularly polarized soft X-Ray high harmonics for X-Ray magnetic circular dichroism. *CLEO 2015 Postdeadline Papers Digest* JTh5C.1 (2015).
26. Milošević, D. Generation of elliptically polarized attosecond pulse trains. *Opt. Lett.* **40,** 2381–2384 (2015).
27. Vincenti, H. & Quéré, F. Attosecond lighthouses: how to use spatiotemporally coupled light fields to generate isolated attosecond pulses. *Phys. Rev. Lett.* **108,** 113904 (2012).
28. Quéré, F. *et al.* Applications of ultrafast wavefront rotation in highly nonlinear optics. *J. Phys. B* **47,** 124004 (2014).
29. Heyl, C. M. *et al.* Noncollinear optical gating. *New J. Phys* **16,** 052001 (2014).
30. Louisy, M. *et al.* Gating attosecond pulses in a noncollinear geometry. *Optica* **2,** 563–566 (2015).

31. Bertrand, J. B. *et al.* Ultrahigh-order wave mixing in noncollinear high harmonic generation. *Phys. Rev. Lett.* **106,** 023001 (2011).
32. Ivanov, M. & Pisanty, E. High-harmonic generation: taking control of polarization. *Nature Photon.* **8,** 501–503 (2014).
33. Pisanty, E., Sukiasyan, S. & Ivanov, M. Spin conservation in high-order-harmonic generation using bicircular fields. *Phys. Rev. A* **90,** 043829 (2014).
34. Mancuso, C. A. *et al.* Strong-field ionization with two-color circularly polarized laser fields. *Phys. Rev. A* **91,** 031402(R) (2015).
35. Durfee, C. G. *et al.* Phase matching of high-order harmonics in hollow waveguides. *Phys. Rev. Lett.* **83,** 2187 (1999).
36. Eichmann, H. *et al.* Polarization-dependent high-order two-color mixing. *Phys. Rev. A* **51,** R3414–R3417 (1995).
37. Long, S., Becker, W. & McIver, J. Model calculations of polarization-dependent two-color high-harmonic generation. *Phys. Rev. A* **52,** 2262–2278 (1995).
38. Boeglin, C. *et al.* Distinguishing the ultrafast dynamics of spin and orbital moments in solids. *Nature* **465,** 458–461 (2010).
39. Höchst, H., Zhao, D. & Huber, D. L. $M_{2,3}$ magnetic circular dichroism (MCD) measurements of Fe, Co and Ni using a newly developed quadruple reflection phase shifter. *Surf. Sci.* **352–354,** 998–1002 (1996).
40. Valencia, S. *et al.* Faraday rotation spectra at shallow core levels: 3*p* edges of Fe, Co, and Ni. *New J. Phys.* **8,** 254 (2006).
41. Yuan, K. J. & Bandrauk, A. D. Single circularly polarized attosecond pulse generation by intense few cycle elliptically polarized laser pulses and terahertz fields from molecular media. *Phys. Rev. Lett.* **110,** 023003 (2013).
42. Yuan, K.-J. & Bandrauk, A. D. Attosecond-magnetic-field-pulse generation by coherent circular molecular electron wave packets. *Phys. Rev. A* **91,** 042509 (2015).
43. Popmintchev, T., Chen, M.-C., Arpin, P., Murnane, M. M. & Kapteyn, H. C. The attosecond nonlinear optics of bright coherent X-ray generation. *Nature Photon.* **4,** 822–832 (2010).
44. Ding, C. *et al.* High flux coherent super-continuum soft X-ray source driven by a single-stage, 10mJ, Ti:sapphire amplifier-pumped OPA. *Opt. Express* **22,** 6194–6202 (2014).
45. Popmintchev, D. *et al.* Ultrahigh-efficiency high harmonic generation driven by UV lasers. *CLEO 2013 OSA Technical Digest* QW1A.5 (2013).
46. Ferrari, F. *et al.* High-energy isolated attosecond pulses generated by above-saturation few-cycle fields. *Nature Photon.* **4,** 875–879 (2010).

Acknowledgements

This work was completed at JILA. D.H., J.E., T.F., K.D., H.C. and M.M. acknowledge support from the Department of Energy BES Award DE-FG02-99ER14982. M.M., H.K. and C.D. acknowledge support from the National Science Foundation's Engineering Research Centre in Extreme Ultraviolet Science and Technology. C.D. acknowledges support from the Air Force Office of Scientific Research under MURI grant FA9550-10-1-0561. J.E. acknowledges support from the National Science Foundation Graduate Research Fellowship (DGE-1144083). C.H.-G. acknowledges support from a Marie Curie International Outgoing Fellowship within the EU Seventh Framework Programme for Research and Technological Development (2007–2013), under REA grant agreement no. 328334. C. H.-G. acknowledges support from Junta de Castilla y León (Project SA116U13) and MINECO (FIS2013-44174-P). A.J.-B. was supported by grants from the National Science Foundation (grants nos. PHY-1125844 and PHY-1068706). This work made use of the Janus supercomputer, which is supported by the National Science Foundation (award no. CNS-0821794) and the University of Colorado, Boulder. P.G. acknowledges support from the Deutsche Forschungsgemeinschaft (grant no. GR 4234/1–1). R.K. acknowledges the Swedish Research Council (VR) for financial support. A.B. acknowledges support from the Department of Energy, Office of Basic Sciences.

Author contributions

C.D., D.H., F.D., M.M. and H.K. conceived the NCP-HHG experiment. P.G., R.K., D.Z. and C.G. designed the MCD experiment. J.S. fabricated and characterized the magnetic sample. D.H., F.D., J.E., K.D., P.G., R.K., D.Z., C.G. and T.F. conducted the experiments. C.H.-G., C. D., A.J.-B. and A.B. conducted and interpreted the numerical simulations of HHG, including propagation. D.H., C.D., F.D., P.G., M.M., H.K. and C.H.-G. wrote the manuscript.

Additional information

Supplementary information is available in the online version of the paper. Reprints and permissions information is available online at www.nature.com/reprints. Correspondence and requests for materials should be addressed to D.D.H.

Competing financial interests

The authors declare no competing financial interests.

Methods

Non-collinear HHG experiment. The apparatus for the generation of circularly polarized HHG light consisted of a Mach–Zehnder interferometer, which focused two laser pulses into a gas jet in a non-collinear geometry. The laser was a Ti:sapphire regenerative amplifier (KMLabs Wyvern-HE) operating at 1 kHz with a 45 fs pulse duration and a central wavelength of 795 nm (referred to as '800 nm'). A pulse energy of 200–400 μJ in each arm was typically used for HHG in argon gas. The laser pulses were focused with the same lens ($f = 250$ mm) into the gas jet.

Circularly polarized HHG was demonstrated using four wavelength combinations: 800 + 800, 800 + 400, 400 + 400 and 267 + 267 nm. The second harmonic of the fundamental (400 nm) was generated using a 200-μm-thick beta barium borate (BBO) crystal. The third harmonic of the fundamental (267 nm) was generated by four-wave mixing of the 400 and 800 nm beams in a second BBO crystal (Eksma Optics). Half and quarter achromatic waveplates placed in each arm of the interferometer were used to manipulate the polarization and produce left and right circularly polarized laser pulses. The peak intensity in the overlapping beams was similar to that required in single beam HHG, $\sim 1 \times 10^{14}$ W cm^{-2} for argon. The two non-collinear beams have a half-angle separation of 1.25–2.5° (25–50 mrad) and were overlapped over a 150-μm-diameter gas jet nozzle. The HHG media were argon and neon gas, with backing pressures between 100 and 300 kPa. The generated EUV light propagated in vacuum (<0.1 Pa) and passed through a 200 nm aluminium filter (Luxel) before being dispersed using a grating-based spectrograph (Hettrick Scientific) and recorded using a back-illuminated X-ray CCD camera (Andor Newton DO920N-BN-9HC). The EUV emission was easily observable even with short exposure times (the longest exposure time used in this study was only 10 s).

EUV MCD measurement. The sample for the EUV MCD experiment was prepared by first sputtering 5 nm germanium onto a 500-nm-thick unsupported aluminium filter. On top of the germanium, 20 nm untextured iron was deposited, which formed the actual magnetic sample to be measured. The iron layer was capped with another 5 nm germanium to prevent oxidation. For the MCD measurement, an electromagnet was used to apply a 15 mT magnetic field for saturating and switching the magnetization of the sample (Supplementary Fig. 5). After collecting a 10 s exposure, the sample magnetization was switched and the data collection was repeated for a total of 90 exposures in each field direction.

The resonant magneto-optical effect can be described as helicity-dependent absorption in a magnetic material, where the imaginary (absorptive) part of the refractive index $n_\pm$ of the magnetically saturated material is given by $\mathrm{Im}(n_\pm) = \beta \pm \Delta\beta$, with β denoting the average absorption coefficient and $\Delta\beta \sim P_{\mathrm{circ}} m\cos\alpha$ the dichroic contribution for opposing photon helicities (±), where P_{circ} is the degree of circular polarization of the light and $m\cos\alpha$ is the projection of the magnetic moment in the direction of the incident light[47,48]. Thus, the MCD asymmetry can be measured by switching the magnetic field with an external electromagnet. To this end, a 20-nm-thick iron sample was inserted at an angle of incidence α of 45° into the HHG beams (Supplementary Section 6). The in-plane magnetization of the sample was switched with an electromagnet and the integrated signal from opposing sample magnetizations was recorded with an X-ray CCD camera.

Theoretical HHG simulations including propagation. The harmonic propagation was computed using a method based on the electromagnetic field propagator[49]. The target (gas jet) was discretized into elementary radiators and propagated the emitted field $\mathbf{E}_j(\mathbf{r}_\mathrm{d},t)$ to the detector,

$$\mathbf{E}_j(\mathbf{r}_\mathrm{d},t) = \frac{q_j \mathbf{s}_\mathrm{d}}{c^2\left|\mathbf{r}_\mathrm{d}-\mathbf{r}_j\right|}\left[\mathbf{s}_\mathrm{d}\times\mathbf{a}_j\left(t-\frac{\left|\mathbf{r}_\mathrm{d}-\mathbf{r}_j\right|}{c}\right)\right]$$

where q_j is the charge of an electron, $\mathbf{s}_\mathrm{d}$ is the unitary vector pointing to the detector, and $\mathbf{r}_\mathrm{d}$ and $\mathbf{r}_j$ are the position vectors of the detector and the elementary radiator j, respectively. The dipole acceleration $\mathbf{a}_j$ of each elementary source was computed using the SFA+ method[50], an extension of the strong field approximation[51–53]. The signal at the detector was computed as the coherent addition of the HHG contributions of all elementary sources, with the HHG light assumed to propagate to the detector with phase velocity c. The propagation effects of the fundamental field, including plasma and neutral dispersion as well as time-dependent group velocity walk-off, were all taken into account. The absorption of the harmonics in the gas was modelled using Beer's law. The attosecond pulses were computed by Fourier transformation of the harmonic spectrum detected at a particular angle after filtering out the low-energy portion (lower than the ninth harmonic order of the fundamental).

Simulations were performed for 800 + 800 and 400 + 400 nm counter-rotating non-collinear mixing, with 32 and 64 mrad crossing angles, respectively. The laser pulse envelopes were modelled by a $\sin^2$ function truncated at the first zeros, with a peak intensity of 8.75×10^{13} W cm^{-2} at the focus for each beam. Various pulse durations were simulated to investigate the role of pulse duration in the HHG process. Each non-collinear driving beam was assumed to have a Gaussian spatial profile (with a beam waist of 40 μm) and taken directly as an input to the calculations. The target was modelled as an argon gas jet flowing perpendicular to the longitudinal direction z. The gas jet profile was constant in the x direction, but Gaussian in the y and z directions, with full-width at half-maximum (FWHM) values of 40 and 20 μm, respectively, and a peak pressure of 667 Pa. Note that the width of the gas jet along the z direction was sufficiently small to assume linear polarization of the total electric field along the target.

Note. The suppliers of commercial equipment, instruments or materials are identified in this Article to foster understanding. Such identification does not imply recommendation or endorsement by the National Institute of Standards and Technology, nor does it imply that the materials or equipment identified are necessarily the best available for the purpose.

References

47. Oppeneer, P. M. *Handbook of Magnetic Materials* (Elsevier, 2001).
48. Stohr, J. & Siegmann, H. C. *Magnetism: From Fundamentals to Nanoscale Dynamics* (Springer, 2006).
49. Hernández-García, C. *et al.* High-order harmonic propagation in gases within the discrete dipole approximation. *Phys. Rev. A* **82,** 033432 (2010).
50. Pérez-Hernández, J. A., Roso, L. & Plaja, L. Harmonic generation beyond the strong-field approximation: the physics behind the short-wave-infrared scaling laws. *Opt. Express* **17,** 9891–9903 (2009).
51. Keldysh, L. V. Ionization in the field of a string electromagnetic wave. *Sov. Phys. JETP* **20,** 1307–1314 (1965).
52. Faisal, F. H. M. Multiple absorption of laser photons by atoms. *J. Phys. B* **6,** L89–L92 (1973).
53. Reiss, H. R. Effect of an intense electromagnetic field on a weakly bound system. *Phys. Rev. A* **22,** 1786–1813 (1980).